COMPUTATIONS OF SWIRLING REACTING FLOW IN A CAN-TYPE COMBUSTOR

P. Di Martino*, G. Cinque**
Alfa Romeo Avio S.A.p.A.
Research and Development Department
80038 Pomigliano d'Arco (NA) ITALY

ABSTRACT

This study is concerned with calculation of steady three-dimensional turbulent reactive swirling flow in a can-type gas turbine combustion chamber. A computational fluid dynamic (CFD) home code based on a pressure-correction methodology combined with the k-ε model has been used. Two combustion models have been chosen and discussed. The former utilizes a conserved scalar formulation (fast chemistry) and an assumed shape probability density function to account for chemistry-turbulence interaction. The latter consists of a two-step global oxidation mechanism with finite rate effects computed using a modified eddy-breakup technique. The numerical algorithm employs structured non-orthogonal body-fitted mesh, node-centered variable arrangement and Cartesian velocity components.

Comparisons between numerical predictions and available experimental data show that CFD is valuable in describing the physics of reactive flows with fairly good accuracy and can be used as a tool to analyze combustion systems.

LIST OF SYMBOLS

B	collision-frequency factor
C_μ	constant of turbulence model
f	mixture fraction
k	kinetic energy of turbulence
J	Jacobian
P(f)	probability density function
q_{ij}	functions of the metrics in equation (2)
S_ϕ	source term
T	gas temperature
T_a	activation energy
u	velocity component (x-direction)
U	contravariant velocity component (ξ-direction)
v	velocity component (y-direction)
V	contravariant velocity component (η-direction)
w	velocity component (z-direction)
W	contravariant velocity component (ζ-direction)

Greek symbols

Γ_ϕ	$= \mu_{eff}/\sigma_\phi$ transport property in equation (1)
ε	dissipation rate of k
ζ	curvilinear coordinate
η	curvilinear coordinate
μ_g	gas laminar viscosity
μ_t	turbulent viscosity
μ_{eff}	$= \mu_t + \mu_g$ effective turbulent viscosity
ξ	curvilinear coordinate
ρ	gas density
σ_ϕ	effective Prandtl/Schmidt number
φ	generalized dependent variable

INTRODUCTION

New design of gas turbine combustors are aimed at simultaneous improvements in several performance parameters. High priority is usually given to expansion of the range of stable operating conditions, improvement of exit temperatures profiles and reduced pollutant emissions. All of these features are crucially dependent on internal flow patterns and the associated rates of mixing. This fact alone has motivated the need for a better and more fundamental understanding of the processes taking place inside a combustion chamber. The design techniques currently in general use are still largely based on costly and lengthy experimental procedures. Whilst this approach has been reasonably successful, increased use of computational procedures in parallel to experimentation would be expected to accelerate the development of improved combustor designs and reduce development costs. This is

---

* CFD Research Manager
** CFD Research Engineer, AIAA Member

particularly evident in view of the fact that the flow characteristics are complicated by non-linear interactions between chemical and fluid dynamic processes. Practical combustion chambers often have complex flowfields to enhance flame characteristics due to the introduction of swirling inlet flow. The strong favorable effects of applying swirl are extensively used as an aid to flame stabilization and promotion of rapid mixing. The predictions of turbulent, swirling, reacting flows found in gas turbine combustion chambers have received considerable attention (Gupta et al., 1984).

In this study we present a CFD computer code based on finite-volume method and body-conforming non-orthogonal but structured grids for calculating steady three dimensional turbulent reactive flows in practical combustors.

A model can-type combustion chamber, intended to be representative of aircraft turbine combustor, was analyzed and numerical results have been compared with measurements of temperature and chemical species.

GOVERNING EQUATIONS

The three-dimensional, steady, fully elliptic, density-weighted Navier-Stokes equations for a reacting gas are considered. Turbulence is simulated by way of the standard k-ε model along with the wall function treatment for the near wall regions, despite the fact that the assumptions involved in this gradient-transport model have very little justification in the complex flow occurring in gas-turbine combustors. However, alternative approaches such as Reynolds stress closure do not yet represent, at present time, viable substitutes in view of the large overhead in CPU time. The transport equations for all dependent variables are of the following form in cartesian coordinates:

$$\left[\frac{\partial}{\partial x}(\rho u\phi) + \frac{\partial}{\partial y}(\rho v\phi) + \frac{\partial}{\partial z}(\rho w\phi)\right] = \left[\frac{\partial}{\partial x}\left(\Gamma_\phi\frac{\partial\phi}{\partial x}\right)+\frac{\partial}{\partial y}\left(\Gamma_\phi\frac{\partial\phi}{\partial y}\right)+\frac{\partial}{\partial z}\left(\Gamma_\phi\frac{\partial\phi}{\partial z}\right)\right]+S_\phi \quad (1)$$

where μ_{eff} is the effective turbulent viscosity, σ_ϕ is the effective Prandtl/Schmidt number. All terms which arise in addition to convection and diffusion are grouped in the source-term S_ϕ.

In order to treat complex shaped domains, the cartesian form of the transport equations must be transformed into a general curvilinear coordinate system. The option followed here is to retain the cartesian decomposition of the velocity vector and just transform the coordinates (x,y,z) to a general non-orthogonal (ξ,η,ζ) set. The transport equation for any scalar property φ (including the individual cartesian velocity components) may then be written (Burns, 1987):

$$\begin{aligned}&\frac{\partial}{\partial\xi}(\rho U\phi)+\frac{\partial}{\partial\eta}(\rho V\phi)+\frac{\partial}{\partial\zeta}(\rho W\phi)=\\&\frac{\partial}{\partial\xi}\left(\frac{\Gamma}{J}q_{11}\frac{\partial\phi}{\partial\xi}\right)+\frac{\partial}{\partial\eta}\left(\frac{\Gamma}{J}q_{12}\frac{\partial\phi}{\partial\eta}\right)+\frac{\partial}{\partial\zeta}\left(\frac{\Gamma}{J}q_{13}\frac{\partial\phi}{\partial\zeta}\right)+\\&\frac{\partial}{\partial\xi}\left[\frac{\Gamma}{J}\left(q_{12}\frac{\partial\phi}{\partial\eta}+q_{13}\frac{\partial\phi}{\partial\zeta}\right)\right]+\frac{\partial}{\partial\eta}\left[\frac{\Gamma}{J}\left(q_{21}\frac{\partial\phi}{\partial\xi}+q_{23}\frac{\partial\phi}{\partial\zeta}\right)\right]+\\&\frac{\partial}{\partial\zeta}\left[\frac{\Gamma}{J}\left(q_{31}\frac{\partial\phi}{\partial\xi}+q_{32}\frac{\partial\phi}{\partial\eta}\right)\right]+JS_\phi(\xi,\eta,\zeta)\end{aligned} \quad (2)$$

In the foregoing mathematical expression U,V,W are the so-called contravariant velocity components, J is the Jacobian of the coordinate transformation, q_{ij} are functions of the metrics, terms with i≠j accounting for grid distortion, and S_ϕ is now the source term in the transformed space. S_ϕ contains, for example, pressure gradients in the case of the velocity components, generation and dissipation terms in the case of the turbulence and cross-derivative diffusion terms for all φ's. There are several approaches for modelling the combustion in turbulent flows. In this study we have chosen two different models: the former uses the assumption of fast chemistry or chemical equilibrium, which enables (coupled with additional hypotheses of low Mach number, equal diffusivities and adiabatic flow) to reduce the instantaneous value of any state variable to a function of a single conserved scalar, which is chosen to be the mixture fraction (Jones et al., 1982). Mean values are obtained by convoluting the instantaneous values with a probability density function (pdf) of presumed shape in terms of two parameters which are evaluated by solving transport equations for the first two moments (mean and variance) of the mixture fraction:

$$\phi = \int_0^1 \phi^e(f)P(f)df \quad (3)$$

where $\phi^e(f)$ is the chemical equilibrium value of φ as a function of f and P(f) is the density weighted p.d.f. for the scalar f. The two-parameter β-function was assumed as p.d.f. (Jones et al., 1982):

$$P(f)=\frac{f^{a-1}(1-f)^{b-1}}{\int_0^1 f^{a-1}(1-f)^{b-1}df} \quad (4)$$

where a and b depend on the mixture fraction and its variance (Jones et al., 1982).

An equation is also solved for stagnation enthalpy from which the temperature field can be extracted through equating the total specific enthalpy to the sum of the species enthalpy. The density of the gas is updated as a function of pressure and temperature using the ideal gas law.

The computation of the integral (3) at all grid points and at each computational step is very time consuming when performed by numerical quadrature. In this study a procedure is adopted which avoids such a quadrature via a convenient formulation, thus reducing the CPU time.

The second approach to turbulent combustion modelling which has been used in this work is based on Arrhenius and Eddy Dissipation Concepts (EDC) (Magnussen et al., 1976). This model is similar to the eddy-breakup type of models. The most important difference between the two is that EDC takes into account that reaction can occur only where both fuel and oxidizer coexist and temperature is high. This is done by relating the reaction rate to the limiting species. Both combustion models have been used to test their capability in predicting chemical species and temperature. The heat release model is given by a one-step irreversible reaction (infinitely fast chemistry) and the following two-step scheme, which allows for calculation of CO (finite rate kinetics):

$$C_xH_y + (0.5x + 0.25y)O_2 \rightarrow xCO + 0.5yH_2O$$

$$CO + 0.5O_2 \rightarrow CO_2$$

NO_x ADVANCED MODELLING

Pollutant emissions, namely NO_x, result from chemical non-equilibrium, i.e. mean formation and destruction rates which are not fast compared with flow processes. Where the effects of finite rate chemistry are thermally insignificant, as in the case of nitrogen oxides which are present in trace amounts, the computation of pollutant concentration can be undertaken as a post-process super-imposing the production mechanism on an established flowfield. The influence of turbulent fluctuations in trace species composition must be accommodated in this mechanism, however, in addition to the fluctuating temperature field. The single scalar probability density function pdf is therefore a constraining factor in even the simplest representations of pollutant chemistry, as in the case for the NO formation.

There are three separate routes to NO production: thermal, prompt and nitrous-oxide mechanism. The prompt pathway is excluded since its contribution is considered negligible.

The extended Zeldovitch mechanism is considered for the thermal NO formation. The initiating an rate determining steps are:

$$N_2 + O = NO + N \qquad \text{(Zeldovitch)}$$

$$N_2 + O + M = N_2O + M \qquad \text{(nitrous oxide)}$$

with M denoting any third body.

Both these rates require the knowledge of the [O] concentration, which is determined from a steady state assumption. The hydrogen-oxygen shuffle steps:

$$OH + H_2 = H_2O + H \qquad (5)$$

$$H + O_2 = OH + O \qquad (6)$$

dominate that state, thereby relating [O] to [H] and concentrations of major species. To eliminate [H] and [OH] partial equilibria are used for the reactions (5) and (6), giving the following expressions for the [O] concentration:

$$[O] = K_1K_2[H_2][O_2]/[H_2O]$$

where K_1 and K_2 are the equilibrium constants for the shuffle reactions (5) and (6). It was further assumed that the ratio $[H_2O]/[H_2] = 5$, which is consistent with diffusion flame reaction zone results available in literature (Rokke et al., 1992). Consequently the NO formation rate can be written in the form:

$$S_{NO} = BT^{\alpha}\exp(-T_a/T)\rho^2 Y_O Y_{N_2} \qquad (7)$$

where B, α, T_a can be found in (Jones, 1980).

The values of S_{NO} are obtained as function of mixture fraction from the equilibrium calculations, so that the instantaneous source term is a function of f only. Its mean value may thus be calculated from (3) in the infinitely fast chemistry model. When finite rate kinetics model is used, the right hand side of (7) contains the non-equilibrium values and no mean is required.

CALCULATION PROCEDURE

The transport equations, for all dependent variables, are integrated over finite volume cells surrounding the mesh nodes. The Fickian diffusive terms were replaced by their central difference analogues, while a higher order upwind scheme (QUICK) was used for convective terms along with

a boundedness criterion to avoid numerical oscillations. The diffusive contributions arising from the coordinate transformation have been included in the source term.

All the variables are stored at the geometric center of the control volume (node centered arrangement). Consequently the velocity interpolation is needed when the convective velocities at the control volume faces are to be estimated. The node centered arrangement coupled with the use of linear interpolation for internodal variation leads to non-physical oscillations or the so-called red-black checker-board splitting of the pressure field. To overcome this problem, a procedure proposed by Rhie and Chow (1983), which is usually described as momentum interpolation, has been adopted to evaluate cell face mass flux terms from the node centered quantities.

Finally the SIMPLEC method (Patankar, 1980) was used to handle the velocity-pressure coupling with proper underrelaxation and the solution of the individual equations sets was obtained by the strongly implicit procedure of Stone (1968).

BOUNDARY CONDITIONS

The set of boundary conditions used in the present study emerged from a preliminary study. The swirler was simulated by an annular gap with the outer and inner radii identical to the real swirler outer and inner radii. The area reduction caused by the vanes in the real swirler has been taken into account by means of an estimated discharge coefficient (0.65). The swirler flow rate and the effective area, together with plug flow assumption, set the mean value of axial velocity. For higher degrees of swirl, however, the axial velocity distribution deviates considerably from plug flow; the major portion of the flow leaves the orifice near the outer edge. Consequently we have assumed that the axial velocity varies linearly from the inner to the outer radius. The two constants of this linear relationship have been obtained from a linear regression of data illustrated in (Gupta et al., 1984), and the swirl number of experiments (0.73) was used. These two constants have been adjusted to reproduce the given swirler flow rate on the grid mesh. Subsequently we have assumed that tangential velocity w is a linearly increasing function of radius r (w=Ar where A is a constant). The value of the constant A has been found from the integration of the swirl number definition, and this guaranteed that experiments and calculation had the same swirl number. The radial velocity was set to zero. The turbulent kinetic energy and the dissipation rate were found by assuming isotropic turbulence, with an axial turbulence intensity of 1.08 ms^{-1}, and a typical eddy length obtained integrating a relationship suggested by Schlichting (1979). A zero axial gradient was prescribed at the outlet section for all the variables. The primary air is introduced through a swirler consisting of eighteen blades oriented at 45°. Fuel (propane) is introduced through ten 1.7 mm diameter jets uniformly and circumferentially spaced around a 90 degree cone located at the center of the swirler. Primary holes (six in number) 10 mm in diameter, equispaced around the combustor, were located 50 mm downstream of the swirler. A second row of 12 equispaced 10-mm-dia holes was placed a further 80 mm downstream. The chamber geometry and the estimated percentage air flows through the swirler, the secondary and dilution jets are shown in fig. 1.

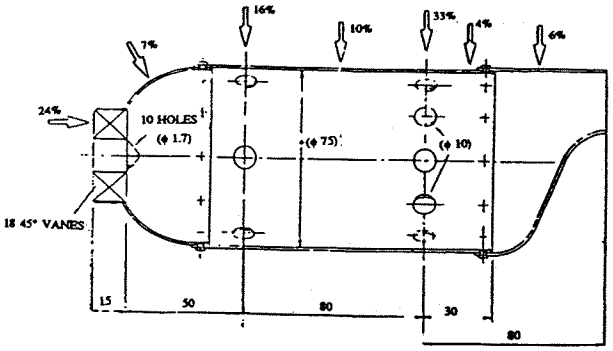

Fig. 1 Combustor geometry.

The fuel injector was simulated by inflow points located in the first column of the grid. A model grid mesh of 51x19x19 (axial, radial, circumferential directions respectively) was used (fig. 2). CPU time required in each of the calculations was about 2 hours on a DEC ALPHA workstation.

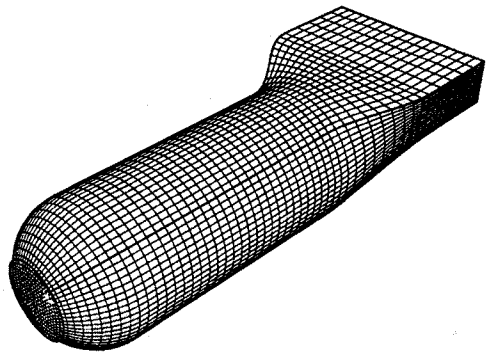

Fig. 2 Three-dimensional view of the model grid mesh.

The mesh was obtained by means of algebraic techniques. Grid-independent solutions are not claimed in this study to

allow a quick turn around with a workstation. The solutions obtained, even in this crudest mesh form, are considered pragmatic from an engineering point of view and as such are satisfactory for their intended purpose. Calculations were performed for two experimental conditions illustrated in table 1.

TABLE 1

	test 1	test 2
Air flow rate (kg/s)	0.085	0.085
Fuel flow rate (g/s)	1.630	1.630
AFR	52.1	52.1
Pressure (atm)	1.	1.
Inlet air temperature (K)	313.	523.

RESULTS AND DISCUSSION

The results of the calculations are shown together with the test data when available (Jones et al. 1983). The velocity vectors in the axial vertical plane through the center of the combustor are illustrated in fig. 3.

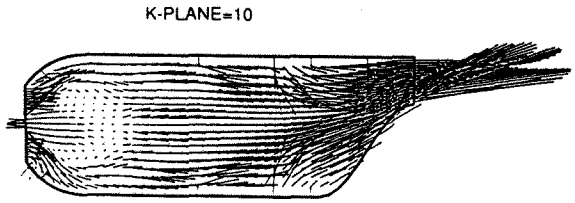

Fig. 3 Calculated flowfield in the axial vertical plane (Kplane=10), test 1.

Note the two contrarotating toroidal vortices in the primary zone, caused by the interaction between the swirler flow and the primary jets, even if the latter are not present in this plane. These vortices probably do not appear at the plane of the primary jets (fig. 4) because of the strong jet impingement.

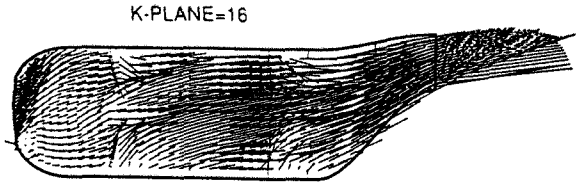

Fig. 4 Calculated flowfield in the plane containing the primary holes (Kplane=16), test 1.

The vortex structure originated by the swirler flow tends to disappear as we move along the combustor axis. This can be observed in fig. 5, where the cross-sectional planes containing the swirler flow, the primary and secondary jets are shown.

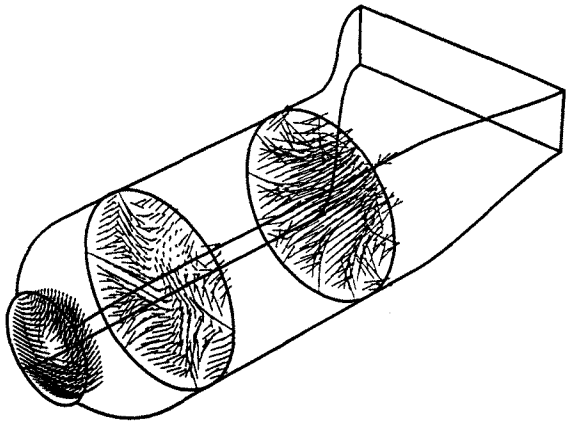

Fig. 5 Calculated flowfield in three cross-sectional planes. Swirl, primary and secondary jets, test 1.

Temperature and chemical species measurements were obtained in a number of points of the exit plane (fig. 6).

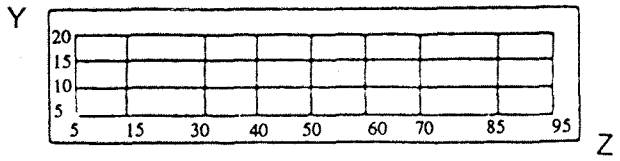

Fig. 6 Measurement grid in the exit plane (dimensions in mm).

The pattern factor (PF) defined as $(T_{max} - T_{av})/(T_{av} - T_{inlet})$, the emission indices defined as the gram weight of CO or UHC per kilogram of fuel have also been measured. Their values are reported in table 2 along with the numerical predictions (finite rate kinetics model).

The calculated emission indices are based on the mean CO and UHC mass fractions which have been obtained by mass averaging the concentration of CO and UHC in the grid points of the exit plane. The mass averaging concept has also been used to evaluate the mean temperature and hence the pattern factor in the exit plane.

A large discrepancy can be observed in the underprediction of EI_{UHC} while EI_{CO} is 20% higher then measured value (test 1). Globally the pattern factor is very close to the test

data.

TABLE 2

	Experiments			Model		
	PF	EI_{UHC}	EI_{CO}	PF	EI_{UHC}	EI_{CO}
test 1	0.720	154	215	0.717	60	262
test 2	0.630	3	87	0.600	0.5	15

The model predicts an excessive quenching of chemical reaction near the outer liner which inhibits CO burnout while UHC is almost completely burned. Some uncertainties of the model are to be found in the values of the constants of EDC combustion model. Globally the prediction is considered reasonable even if reliable absolute emissions values are not yet good. Comments on test 2 will be made in the following.

Figures 7-12 show profiles of CO, UHC, CO_2, O_2, NO_x (all concentrations on wet basis), and temperature in the exit plane respectively, at various y-coordinates (test 1).

The predictions of CO agree quite well with experiments (fig. 7), especially those relative to the lower part of the combustor (Y=5 mm, Y=15 mm).

As far as UHC is concerned (fig. 8), the calculations underpredict the concentrations by almost a factor of 2. The best agreement is observed in the central part of the combustor.

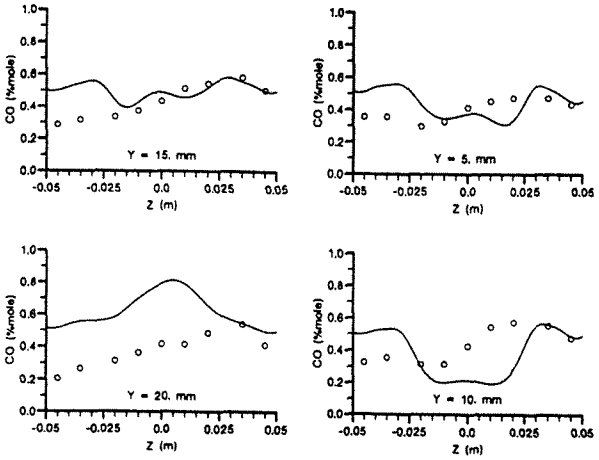

Fig. 7 CO exit plane contours at various y coordinates, (o) exper. (___) model, test 1.

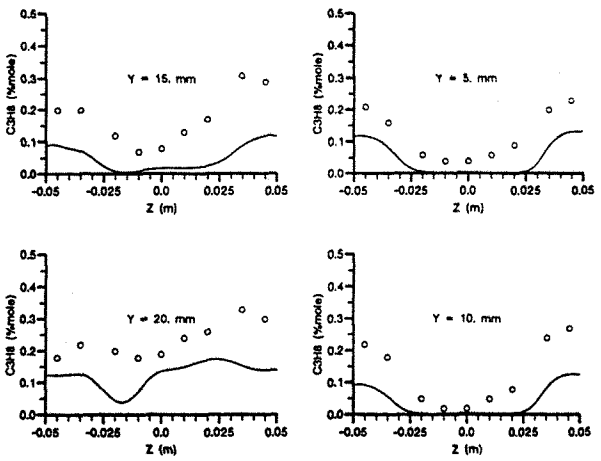

Fig. 8 UHC exit plane contours at various y coordinates, (o) exper. (___) model, test 1.

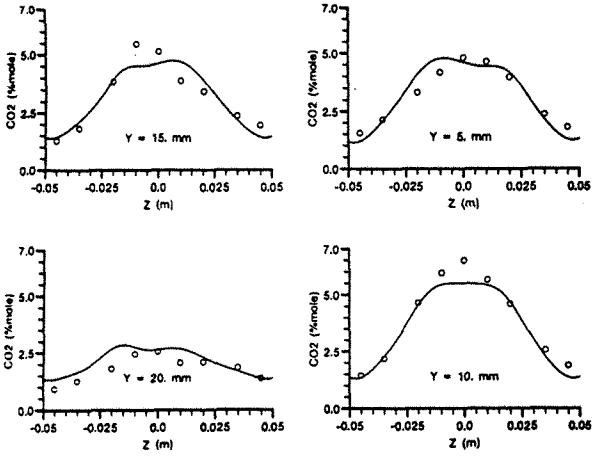

Fig. 9 CO_2 exit plane contours at various y coordinates, (o) exper. (___) model, test 1.

The values of the other chemical species are very close to the test data, as shown in figg. 9-11.

The temperature distribution obtained with the finite rate kinetics model is illustrated in fig. 12. The agreement is reasonable in general with an underprediction in the central

part of the combustor cross section.

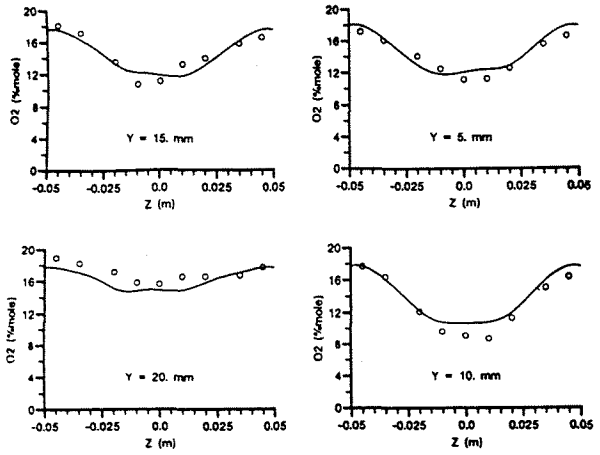

Fig. 10 O_2 exit plane contours at various y coordinates, (o) exper. (___) model, test 1.

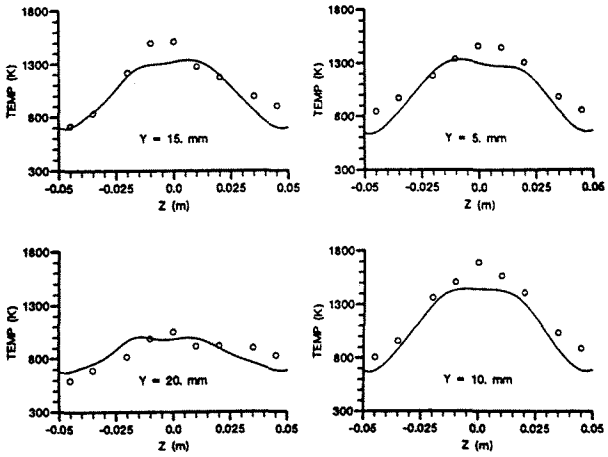

Fig. 12 Temperature exit plane contours at various y coordinates, (o) exper. (___) model, finite rate kinetics model, test 1.

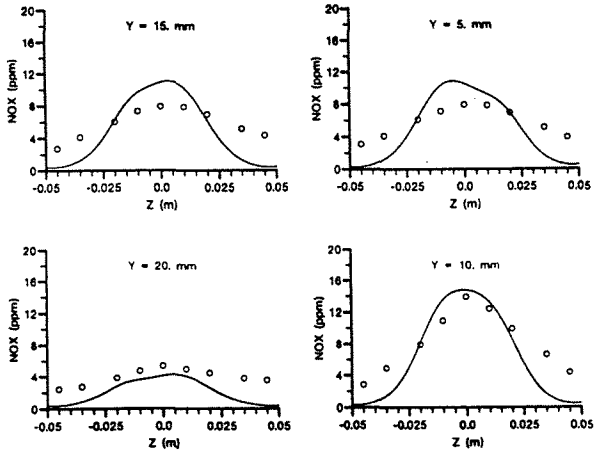

Fig. 11 NO_x exit plane contours at various y coordinates, (o) exper. (___) model, test 1.

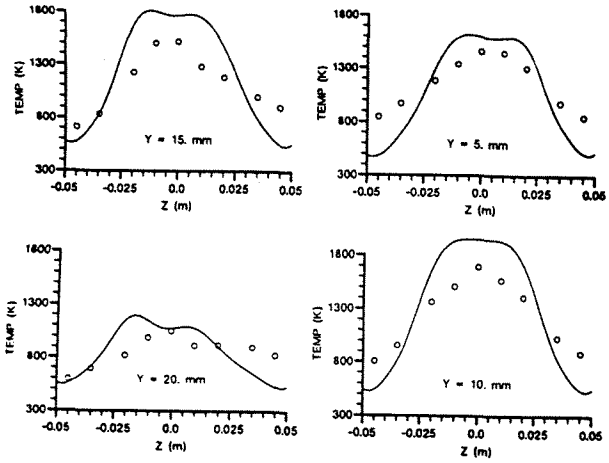

Fig. 13 Temperature exit plane contours at various y coordinates, (o) exper. (___) model, infinitely fast chemistry model, test 1.

In order to compare the two combustion models used in this study, fig. 13 shows the temperature distribution obtained with the infinitely fast chemistry. The trend is only qualitatively good but quantitatively poor.

This clearly indicates that the equilibrium assumptions do not prevail everywhere.

In addition to that there is the failure of turbulence viscosity models in the prediction of recirculating flows, based on the argument that turbulence is mainly generated by the interaction between the fluctuating density and

velocity field, and the mean pressure gradient. It follows that the use of higher order closure turbulence models is needed.

Predictions have also been performed with various values of turbulent Prandtl number. Calculations with a value of 0.4 show smoother distributions (figg. 14-16).

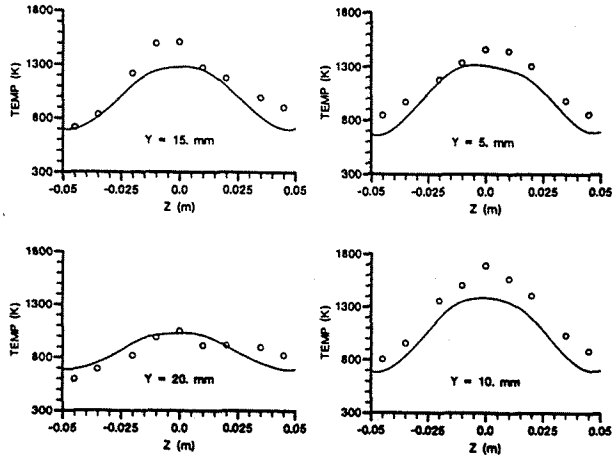

Fig. 14 Temperature exit plane contours at various y coordinates, (o) exper. (___) model, finite rate kinetics, Prandtl=0.4, test 1.

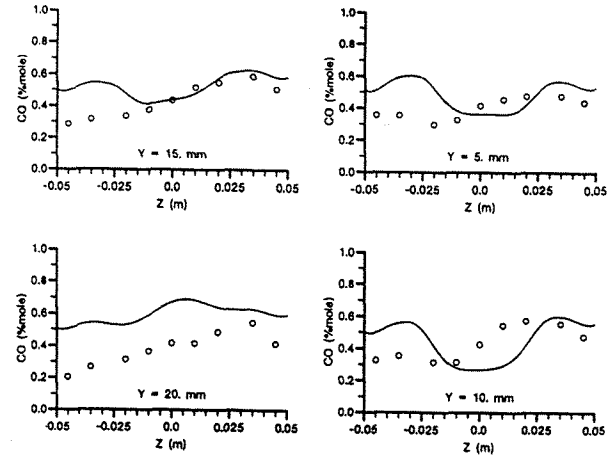

Fig. 15 CO exit plane contours at various y coordinates, (o) exper. (___) model, finite rate kinetics, Prandtl=0.4, test 1.

The need to increase the diffusion of scalars for better agreement with the measurements contrasts with the suggestion to lower the eddy viscosity in order to reduce the high diffusion of momentum, which is known to be a typical feature of the k-ε model.

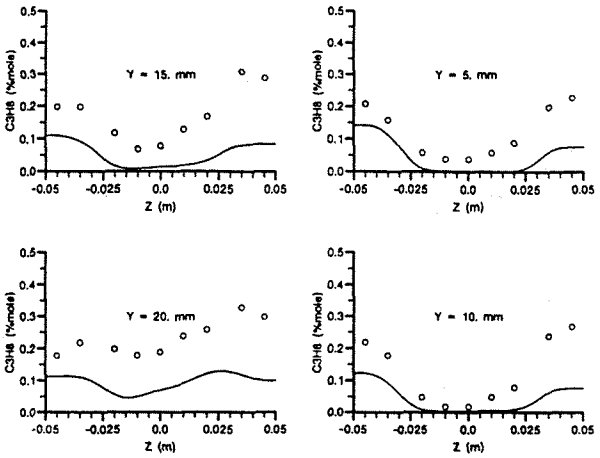

Fig. 16 UHC exit plane contours at various y coordinates, (o) exper. (___) model, finite rate kinetics, Prandtl=0.4, test 1.

The difficulty of selecting the appropriate Prandtl number is the evidence of the deficiency of the scalar flux model, which might be overcome by using higher order scalar flux models to take into account the strong flow anisotropy.

As for test 2, figures 17-20 show exit plane temperature contours, CO_2, O_2 and NO_x concentration respectively.

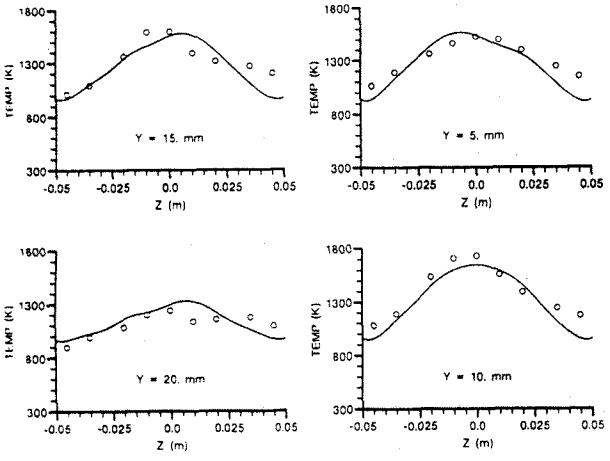

Fig. 17 Temperature exit plane contours at various y coordinates, (o) exper. (___) model, finite rate kinetics, test 2.

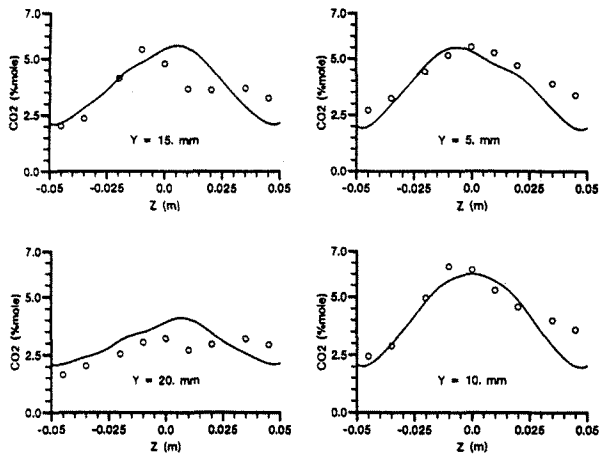

Fig. 18 CO_2 exit plane contours at various y coordinates, (o) exper. (___) model, finite rate kinetics, test 2.

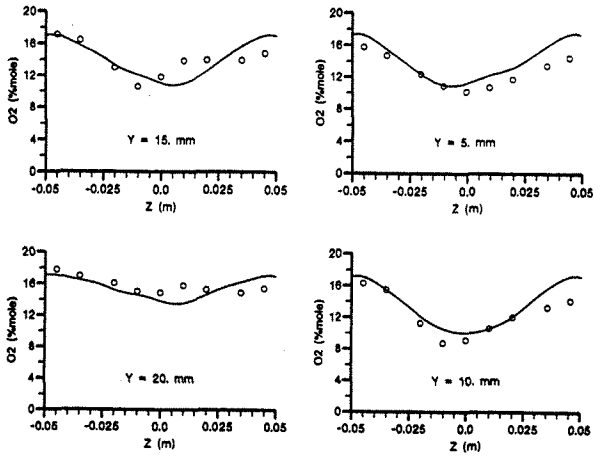

Fig. 19 O_2 exit plane contours at various y coordinates, (o) exper. (___) model, finite rate kinetics, test 2.

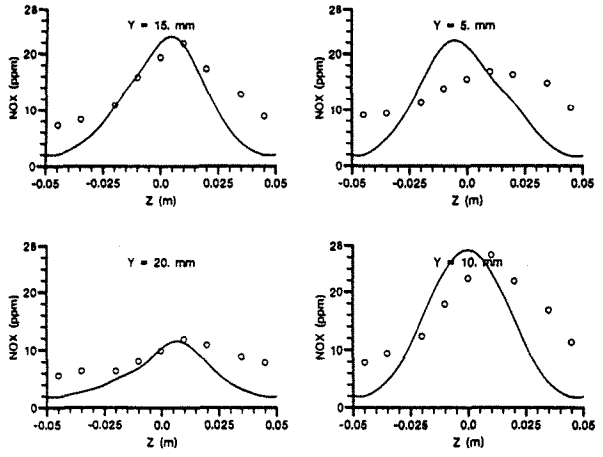

Fig. 20 NO_x exit plane contours at various y coordinates, (o) exper. (___) model, finite rate kinetics, test 2.

Globally the agreement between calculations and experiments is fairly good. Predictions of UHC and CO concentrations have not been reported. The finite rate combustion model indicates that UHC and CO are almost completely burned and this result is consistent with the calculated emission indices which are well below the experimental values (table 2). A further study to improve the combustion model is needed. Among the others, a limit which should be overcome is to link the constants of EDC model to some balance equations of statistical quantities.

CONCLUSION

A typical can-type combustion chamber has been modelled using a three dimensional, body-fitted CFD home code. Calculations were performed for two experimental conditions. The flowfield, chemical species distributions and temperatures within the combustor were computed. The agreement with test measurements can be considered encouraging if not fair, in view of the many interdependent processes involved. Even if a coarse mesh has been used and no grid-independent solutions are claimed, the boundaries of the calculation domain are quite well represented. Turbulence and combustion models need to be improved. In general the predictions of the main chemical species (CO_2, O_2) and temperature are reasonable in both test 1 and test 2. Some uncertainties are to be found in UHC and CO levels. This fact indicates that a three or four step oxidation mechanism (including H_2 formation and destruction) for the fuel is needed and a better model for turbulence-chemistry interaction is necessary. The NO_x prediction can be considered quite satisfactory even if it can be improved using the quoted multistep reaction scheme and the method described above since they will give a reasonable estimate of $[H_2O]/[H_2]$. The numerical modelling of the combustor as presented here showed that although some of the mathematical models have room to improve, CFD techniques illustrated above are capable of providing physically realistic solutions and can be used to get improved understanding of the flow physics in complex combustion systems.

REFERENCES

Burns, A. D., and Wilkes, N. S., 1987, "A Finite Difference Method for the Computation of Fluid Flows on Complex Geometries", AERE-R 12342, Harwell Laboratory, Oxfordshire, U.K..

Gupta, A. K., Lilley, D. G., Syred, N., 1984, Swirl Flows, Abacus Press.

Jones, W. P., 1980, "Models for Turbulent Flows with Variable Density and Combustion", *Prediction methods for turbulent flows,* Kollmann W. ed., Hemisphere, Washington.

Jones, W. P., and Toral H., 1983, "Temperature and Composition Measurements in a Research Gas Turbine Combustion Chamber", *Comb. Sci. and Tech.,* Vol. 31, pp. 249-275.

Jones, W. P., and Whitelaw, J. H., 1982, "Calculation Methods for Turbulent Reacting Flows: a Review", *Comb. Flame,* Vol. 48, pp. 1-26.

Magnussen, B. F., and Hjertager, B. H., 1976, "On Mathematical Modelling of Turbulent Combustion with Special Emphasis on Soot Formation and Combustion", *Sixteenth Symposium (International) on Combustion,* pp. 719-729.

Patankar, S. V., 1980, *"Numerical Heat Transfer and Fluid Flow",* Hemisphere Publishing Co., New York.

Rhie, C. M., and Chow, W. L., 1983, "Numerical Study of the Turbulent Flow Past an Airfoil with Trailing Edge Separation", *AIAA Journal,* vol. 21, no. 11, pp. 1525-1532.

Rokke, N. A., Hustad, J. E., Sonje, O. K., and Williams, F. A., 1992, "Scaling of Nitric Oxide Emissions from Buoyancy Dominated Hydrocarbon Turbulent-jet Diffusion Flames", *Twenty-Fourth Symposium (International) on Combustion,* pp. 385-393.

Schlichting, H., 1979, Boundary-Layer Theory, Mc Graw-Hill (Seventh Edition).

Stone, H. L., 1968, "Iterative Solution of Implicit Approximations of Multidimensional Partial Differential Equations", *SIAM Journal on Numerical Analysis,* Vol. 5, pp. 530-558.